

NiO Thin Film Growth Through Mist CVD Growth Mechanism

Thesis

Presented in Partial Fulfillment of the Requirements for the Degree Master of Science in
the Graduate School of The Ohio State University

By

Taiga Yamawaki

Graduate Program in Electrical and Computer Engineering

The Ohio State University

2024

Thesis Committee

Hongping Zhao

Wladimiro Villarroel

Copyrighted by
Taiga Yamawaki
2024

Abstract

In this thesis, NiO growth via mist CVD technology is reported. Recently beta- Ga₂O₃ is considered as the candidate to be used for future power electronics. However, one of the challenges remaining for beta- Ga₂O₃ is the lack of p-type conductivity. Due to the difficulty of attaining p-type conductivity in β-Ga₂O₃, our research group has focused on the growth of NiO thin films, which offer the advantages of wide bandgap, p-type conductivity, and high productivity, through mist CVD, a method known for its efficiency in producing oxide semiconductors. The mist CVD method is a cost-effective, safe, environmentally friendly, and easily improvable process compared to other thin-film deposition techniques. Mist CVD is a relatively simple process that allows for thin film growth at atmospheric pressure, eliminating the need for specialized equipment like vacuum technology, and its overall structure is straightforward. Additionally, the raw materials used in this method are high-purity reagents, which are low in toxicity and risk. Therefore, if NiO can be deposited using mist CVD, it could enable the development of devices with low environmental impact, low cost, and high productivity. Our research group built a custom mist CVD system from scratch to grow NiO thin films. The system design required knowledge of mist CVD and other CVD techniques, the construction of pipelines for carrier gas, and gas supply cylinders, and the installation of other necessary equipment. Using the constructed system, we repeatedly conducted NiO thin film growth

experiments and based on the collected X-Ray-Diffraction (XRD) data, NiO was successfully grown.

Acknowledgment

I would like to express my deepest gratitude to the members of the Professor Zhao Laboratory Group. It has been an honor to conduct research as part of this group, and their dedication and passion for research have provided me with invaluable experiences. I am especially grateful to Mr. Kaitian for his support with the characterization part and the setup of the mist CVD system. His guidance was instrumental in the completion of my thesis, and I could not have achieved this thesis without his assistance. I would also like to extend my thanks to Dr. Zhao for her insightful guidance in helping me identify and refine my thesis topic. The experiences I have gained at The Ohio State University have been invaluable to me, and I am excited to apply this knowledge in my future career as an engineer.

Vita

August 2019, Hanover College

August 2023 to present, The Ohio State University, Department of Electrical and
Computer Engineering

Fields of Study

Major Field: Electrical and Computer Engineering

Table of Contents

Abstract	ii
Acknowledgment.....	iv
Vita.....	v
List of Tables.....	viii
List of Figures	ix
Chapter 1. Introduction/Background	1
1.1 Thin film.....	1
1.2 Thin film deposition techniques	3
1.3 Mist CVD process	7
1.4 Wide bandgap semiconductor	9
1.5 NiO.....	12
1.6 Purpose of this thesis and structure	14
Reference.....	15
Chapter 2. Theory of mist CVD.....	19
2.1 Mist vs Spray	19
2.2 Mist CVD (equipment and approach)	21
2.3 Theoretical review of Ultrasound wave	24
2.4 Theoretical review of mist particle behavior.....	27
Reference.....	31
Chapter 3 Characterization method.....	32
3.1 X-ray diffraction (XRD)	32
3.2 Hall effect measurement.....	35
3.3 Surface morphology characterization via SEM.....	38
3.4 X-ray Photoelectron Spectroscopy (XPS).....	40
Reference.....	44

Chapter 4 NiO growth.....	46
4.1 Mist CVD process setup.....	46
4.2 Growth conditions/procedure	48
4.3 Result	49
Chapter 5 Conclusion and Future Work.....	52
Bibliography	53

List of Tables

Table 1. The main equipment used in this thesis	47
Table 2. NiO growth condition	48

List of Figures

Figure 1. Thin Film	1
Figure 2. Types of PVD and CVD	3
Figure 3. Process of vapor deposition	4
Figure 4. The periodic table highlighted the materials growth by mist CVD [1.3.3]	8
Figure 5. Semiconductors bandgap energy vs lattice constant [1.4.1]	9
Figure 6. NiO crystal structure [1.5.23]	13
Figure 7. Mist deposition vs spray deposition.....	20
Figure 8. Schematic of mist CVD	21
Figure 9. Range of sound [2.3.1].....	24
Figure 10. Bragg's law	33
Figure 11. Omega-2theta scan.....	34
Figure 12. Hall effect measurement [3.2.1]	35
Figure 13. Schematic of SEM image	39
Figure 14. XPS theory.....	40
Figure 15. Mechanism of photoelectron generation.....	41
Figure 16. Experimental setup	46
Figure 17. Wafer carrier	48
Figure 18. XRD result	49
Figure 19. SEM position 1	50
Figure 20. SEM position 2	50
Figure 21. XPS result	51

Chapter 1. Introduction/Background

1.1 Thin film

The term thin film refers to the film on the substrate which may be a few nanometers to several micrometers [1.1.1]. Figure 1 illustrates the thin film on the substrate.

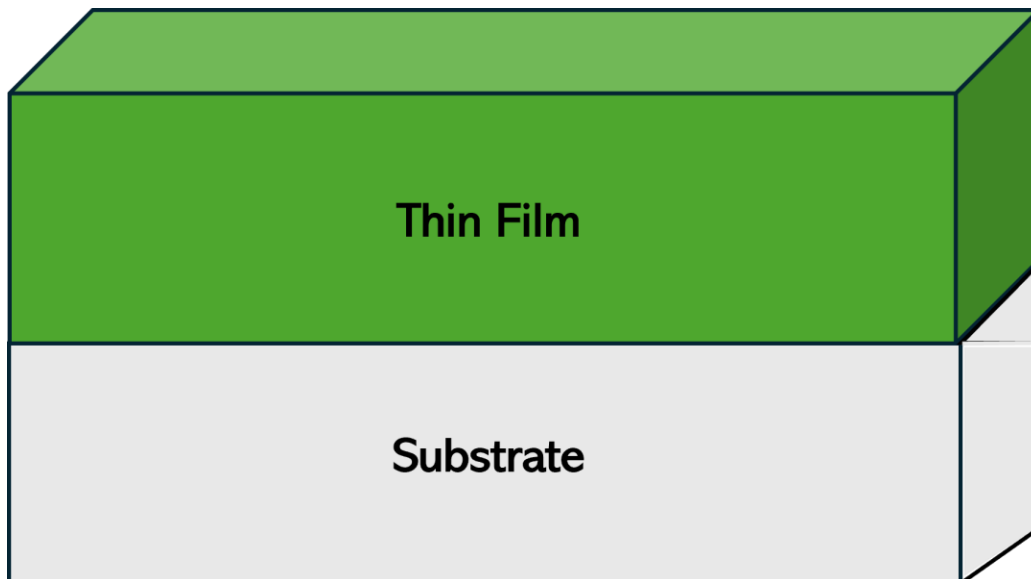


Figure 1. Thin Film

Thin film is used daily and has various characteristics such as electrical, optical, magnetic, thermal, mechanical, and chemical. In recent times, transparent conducting films (TCFs) are the backbones of numerous modern gadgets and are crucial in realizing the future devices involving organic light-emitting devices, smart windows, and touch screens for the flexible wearable [1.1.2]. In optical applications, thin films are used in

antireflection films for camera lenses and cold mirrors for lighting [1.1.3] Each application requires thin films with specific functions, and thus, a wide variety of materials are used. In the semiconductor industry, improvement of the quality of thin film is important for better device performance. Today's technology such as smartphones is the result of the improvement of thin film growth, integrated circuits, nanotechnology, etc. Improvement of thin film growth allows the thinner film and high-quality film which result in the improvement of the performance of the electronic devices.

1.2 Thin film deposition techniques

Thin film deposition techniques are crucial for depositing thin films onto a substrate and there are mainly two types of thin film growth techniques for the vapor deposition process which is commonly used in thin film process technology. These are physical vapor deposition, PVD, and chemical vapor deposition, CVD. The variety of types of PVD and CVD processes are shown in Figure 2.

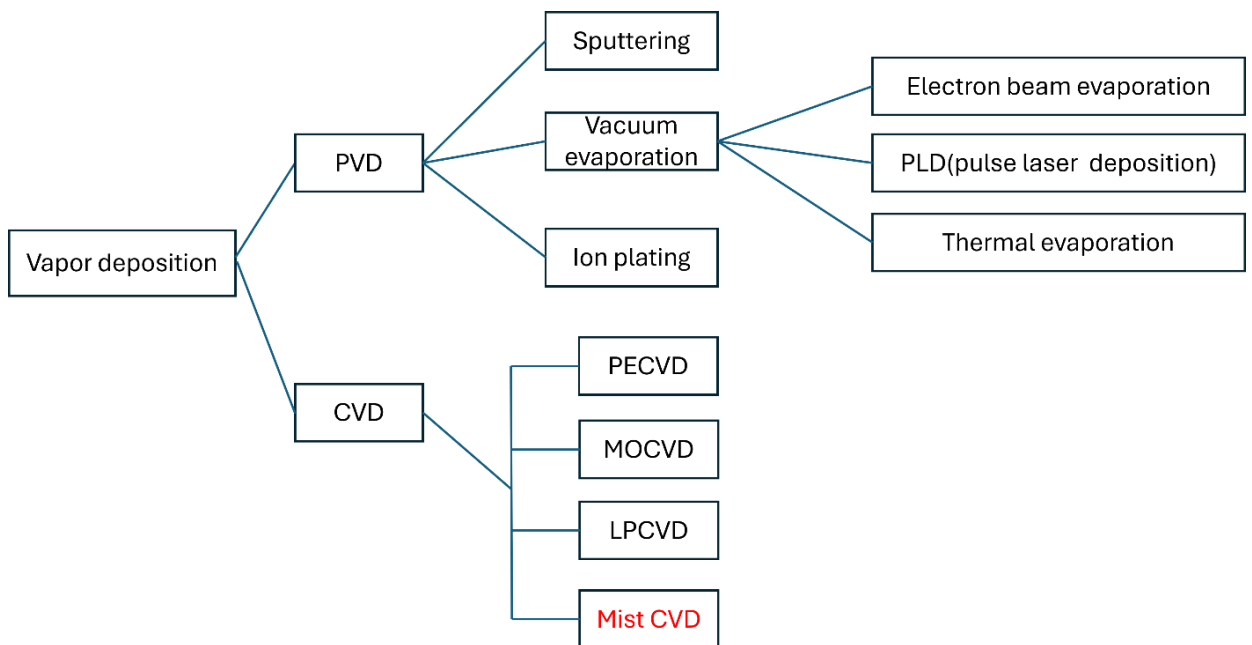


Figure 2. Types of PVD and CVD

Many PVD processes are conducted at pressures lower than atmospheric pressure.

Conversely, CVD operates at much higher pressures than PVD due to the necessity of chemical reactions during the transport process. For those processes, vacuum technology is essential for producing thin films with high reproducibility, durability, and uniformity

over large areas. Regardless of whether the deposition technique is based on vapor phase or liquid phase growth, the general process of thin film deposition consists of three fundamental steps: decomposing the raw material into atoms, molecules, or clusters (decomposition/evaporation process), transporting these to the substrate (transport process), and depositing them onto the substrate surface (deposition process). The key contrast between PVD and CVD lies in how the thin film is placed on the substrate. PVD involves vaporizing the solid material and condensing it onto the substrate, whereas CVD involves the gas or vapor reacting with the substrate to create a solid thin film [1.2.1]. The overall process of the vapor deposition process is shown in Figure 3.

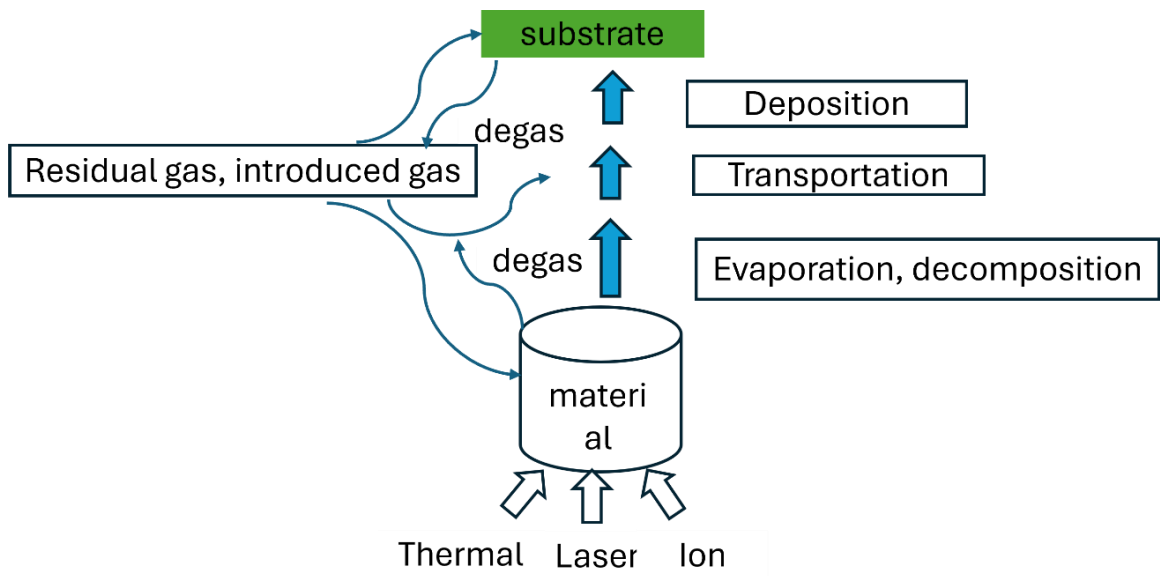


Figure 3. Process of vapor deposition

As shown in Figure 3, the process of vapor deposition is as follows:

Initially, energy sources such as heat, laser, or ion decompose or evaporate the raw material. In the case of CVD, where the raw material is supplied as a gas, this decomposition process may be considered complete at the raw material. The vapor generated in the decomposition/evaporation process is then transported towards the substrate within the apparatus. In PVD, the atoms and molecules ejected from the raw material during decomposition are typically not controlled but are naturally received by the substrate to form a thin film. In CVD, the vapor is mixed with an appropriate carrier gas and transported via the gas flow. During this process, the vapor is energized by heat or plasma to promote chemical reactions. Finally, the vapor or the reaction products deposit onto the substrate to form a thin film. Atoms and molecules adsorbed onto the substrate surface lose their kinetic energy from the transport process and diffuse or migrate across the surface before settling. During this time, chemical reactions may occur to supplement missing components or eliminate excess ones from the vapor, determining the crystallinity and composition of the resulting thin film. To control this process, the substrate may be heated as necessary. The overall process of vapor phase growth for thin films involves these fundamental steps, but there are various variations in the decomposition/evaporation and vapor transport processes, each with different names. As mentioned earlier, most PVD and CVD processes require vacuum technology. The equipment for vacuum processing is expensive and not environmentally friendly. Most of the PVD techniques require the vacuum chamber because they require the generation of electrons and plasma. In CVD, it is necessary to transport metal elements in the gas phase, making materials with high vapor pressure suitable as raw materials. The

disadvantage of the CVD process is that it generates hazardous by-products (toxic, corrosive or explosive), requiring costly health and environmental safeguards [1.2.2]. Additionally, the raw materials used in the CVD process are quite expensive. There are still many issues regarding the efficiency of raw material utilization and the uniformity of the thin films.

1.3 Mist CVD process

Recently, wide bandgap oxide semiconductors such as Ga_2O_3 , NiO , and LiGa_5O_8 are considered candidates to be used for future power electronics and optoelectronics. Unlike arsenide or nitrides, oxide semiconductors are suitable to be fabricated by green chemistry (or green processes), that is, by non-vacuum and solution-based deposition methods, because one does not need to be so nervous about oxygen contamination which is a fatal problem for non-oxide semiconductor materials. From the standpoint of protecting the global environment, it is essential to develop safe raw materials with low environmental impact and deposit technologies that consume less energy in forming thin-film materials. The mist CVD process is known as a cost-effective, safe process, environmentally friendly [1.3.1], and easy to modify among the other thin film deposition techniques. Mist CVD is a relatively straightforward process that grows thin films at atmospheric pressure, requiring no special equipment such as vacuum technology and having a simple structure. It also uses raw materials that are used as high-purity reagents with low toxicity and hazard. In other words, it is a safe, inexpensive, and energy-saving deposition technique with minimal environmental impact. The key feature of this method is its use of micro- and sub-microscale droplets, or "mist," which can be transported as liquid and easily vaporized with slight atmospheric changes, exhibiting both liquid and gas properties. These properties are particularly beneficial for thin film growth and processing.

Another characteristic of mist CVD is that by simply mixing precursor materials that form mixed crystals or dopants into the solution, mixed crystal formation and

impurity addition can be achieved. In the case of the widely used MOCVD, Metal-Organic Chemical Vapor Deposition, method, the precursors need to be vaporized, which imposes vapor pressure constraints. However, in the mist CVD method, where ultrasonic atomization is used, numerous precursor materials can be dissolved in the solution, broadening the range of material selection.

Mist CVD has been under development since around 1980 [1.3.2], but significant advancements began in 2003 when researchers at the Fujita Laboratory at Kyoto University, including the authors, started refining the technique. Their efforts focused on producing uniform thin films over large areas by improving the laminar flow of the mist gas. Figure 4 shows the materials grown by the mist CVD process.

1	2	3	4	5	6	7	8	9	10	11	12	13	14	15	16	17	18
H																	He
Li	Be											B	C	N	O	F	Ne
Na	Mg											Al	Si	P	S	Cl	Ar
K	Ca	Sc	Ti	V	Cr	Mn	Fe	Co	Ni	Cu	Zn	Ga	Ge	As	Se	Br	Kr
Rb	Sr	Y	Zr	Nb	Mo	Tc	Ru	Rh	Pd	Ag	Cd	In	Sn	Sb	Te	I	Xe
Cs	Ba	Lanthanoid	Hf	Ta	W	Re	Os	Ir	Pt	Au	Hg	Tl	Pb	Bi	Po	At	Rn
Fr	Ra	Actinoid	Rf	Db	Sg	Bh	Hs	Mt	Ds	Rg	Cn	Nh	Fl	Mc	Lv	Ts	Og

Figure 4. The periodic table highlighted the materials growth by mist CVD [1.3.3]

1.4 Wide bandgap semiconductor

In the previous section, the benefit of using the mist CVD process for the growth of the thin film of the oxide semiconductor is discussed. Recently, there has been a growing focus on studying wide bandgap semiconductor materials for their potential use in next-generation power electronics and optoelectronic devices. Wide bandgap semiconductors have a larger bandgap than typical semiconductor materials such as silicon (Si: 1.12 eV) and gallium arsenide (GaAs: 1.42 eV). Examples of wide bandgap semiconductors include gallium nitride (GaN: 3.4 eV), zinc oxide (ZnO: 3.3 eV), and silicon carbide (SiC: 3.3 eV). Figure 5 illustrates common binary compound semiconductors' room temperature bandgap energies vs. their lattice constants.

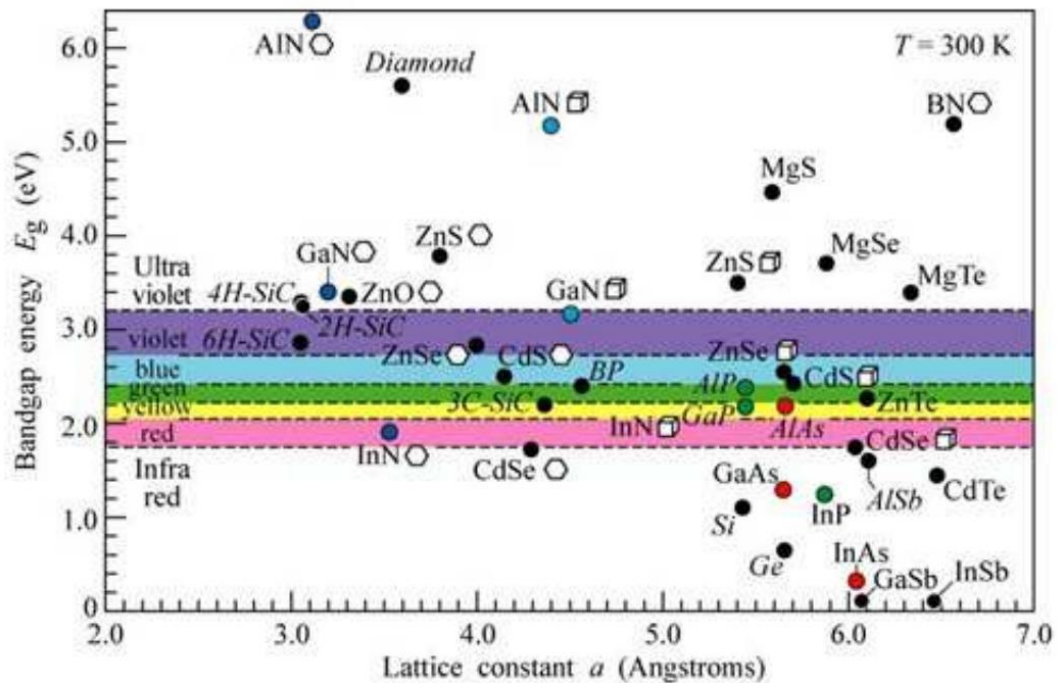


Figure 5. Semiconductors bandgap energy vs lattice constant [1.4.1]

In the semiconductor industry, the wide bandgap semiconductor materials are applicable in power devices and optoelectronic devices for high-frequency and high-voltage applications. They offer superior properties or enable devices that cannot be realized with Si which is the most popular semiconductor material. In the field of optoelectronics, unlike Si, which has a bandgap corresponding to the near-infrared region as can be seen from Figure 5, the wide bandgap semiconductors have emission and absorption properties in the shorter wavelength region, making them suitable for ultraviolet (UV), emission devices, or shorter wavelength region. The equation relating the bandgap energy (E_g) to the wavelength (λ) of the material is given by Equation 1.4.1:

$$E_g = \frac{1240}{\lambda(nm)} eV \quad 1.4.1$$

From Equation 1.4.1, wide bandgap semiconductors can be used for shorter wavelength region applications for optoelectronic devices.

In the power device field, the critical electric field, E_c , roughly estimated by the size of the bandgap is a measure of the material's voltage withstand capability. A performance parameter for power devices called the Baliga figure of merit, BFOM, is expressed as $\epsilon\mu E_c^3$ for low-frequency applications and $\epsilon\mu E_c^2$ for high-frequency applications, where electron mobility: μ (cm^2/Vs), dielectric constant: ϵ (F/cm), and critical electric field: E_c (V/cm). BFOM is determined by physical constants and increases in proportion to E_c^3 or E_c^2 depending on low or high-frequency applications.

Since the breakdown electric field has a positive bandgap coefficient, meaning the breakdown electric field increases with increasing value of bandgap, using wide bandgap

semiconductors enables high-voltage, high-current control with low energy loss. Typical power device applications of wide bandgap semiconductors include field-effect transistors (FET), Schottky barrier diodes (SBD), and high electron mobility transistors (HEMT).

1.5 NiO

Recently, beta gallium oxide (β - Ga₂O₃) has emerged as a candidate for future generation power electronic devices, with ultrawide bandgap (≈ 4.9 eV), [1.5.1-1.5.3] high critical electric field (7– 8 MV cm⁻¹), [1.5.4], n-type doping [1.5.5-1.5.9]. One of the challenges in the practical application of β - Ga₂O₃ is the realization of p-type conductivity. Since achieving p-type for beta β - Ga₂O₃ is difficult, this thesis focuses on NiO as a material that combines the benefits of oxide semiconductors, such as a wide bandgap, p-type conductivity, and high productivity using the mist CVD process. NiO is a wide bandgap oxide semiconductor that has 3.6-4.0 eV [1.5.10] and has characteristics of stability, switchable electrical and optical properties, and p-type conductivity. Due to its excellent electrochemical stability and low material cost, this antiferromagnetic transition metal oxide semiconductor is expected to have various applications in optical and electrical devices. NiO thin film has potential applications such as electrochromic coatings [1.5.11], resistance switching[1.5.12], gas sensing[1.5.13], p-type transparent conductors[1.5.14-15], organic photovoltaics[1.5.16-17], Photocathode for a SolarCell[1.5.18] and Electrochromics for smart windows[1.5.19]. NiO thin film has been grown by several techniques including sputtering [1.5.12-15], chemical solution deposition [1.5.16-17], chemical vapor deposition[1.5.20], atomic layer deposition[1.5.21], and thermal evaporation[1.5.22]. NiO is rare among oxide semiconductors in that it exhibits p-type conductivity. P-type materials are necessary for device applications, making research on NiO growth important. Additionally, if NiO can be deposited using the mist CVD method, it would enable the realization of devices with

low environmental impact, low cost, and high productivity. Figure 6 shows the crystal structure of NiO. Due to a strong electron correlation in 3d orbitals, NiO has an optical bandgap of 3.4–4.0 eV [1.5.23].

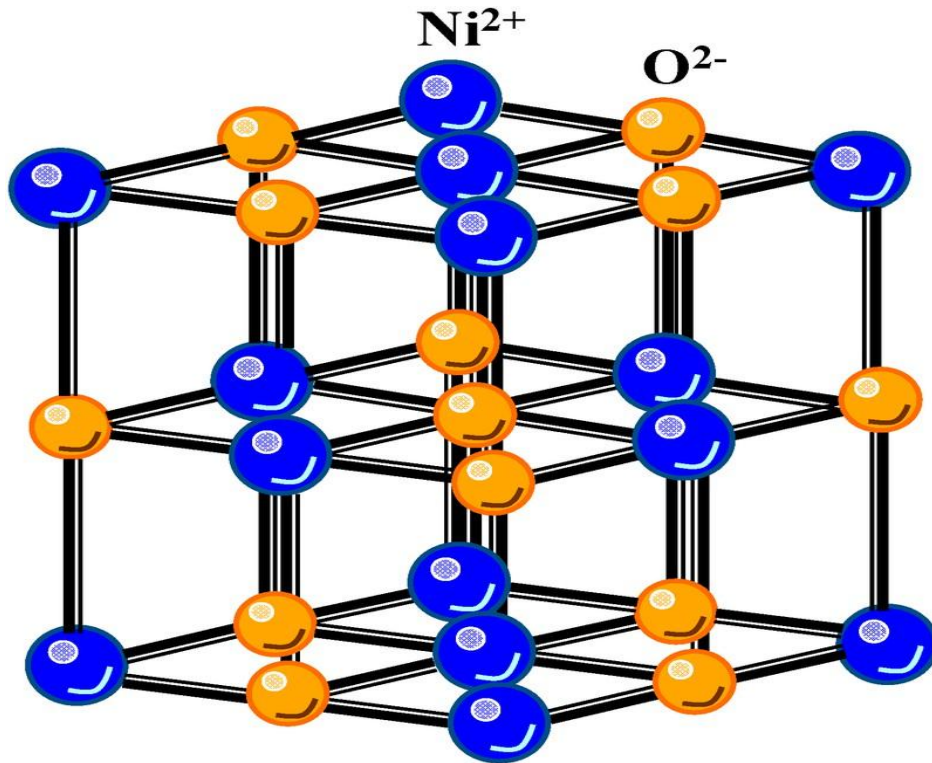


Figure 6. NiO crystal structure [1.5.23]

1.6 Purpose of this thesis and structure

Oxygen makes up 20% of the Earth's atmosphere, and all substances are ultimately oxidized. As a result, many oxide materials are extremely stable on the earth. This thesis focuses on the study of the theory of the mist CVD mechanism and aims to explore the growth of NiO thin film using the mist CVD process. The purpose of this thesis is to establish the fabrication technique for NiO thin film using the mist CVD process and characterize the NiO thin films grown by the mist CVD process. From an environmental perspective, this will certainly contribute to the society. It also serves as a guideline for future thin film growth development and has the potential to be used for future power and optoelectronics device applications. The structure of this thesis is as follows:

In Chapter 2, the theory of the mist CVD technique is discussed. This chapter digs deep into the mechanism and theory behind the mist CVD technique. In Chapter 3, the characterization method used in this thesis is discussed. In Chapter 4, the experimental setup of the mist CVD, the growth condition, and the experimental result of the NiO thin film are discussed. Finally, Chapter 5 discusses the summary of this thesis and the potential future work for this topic.

Reference

- [1.1.1] Kumar, S., Aswal, D.K. (2020). Thin Film and Significance of Its Thickness. In: Kumar, S., Aswal, D. (eds) Recent Advances in Thin Films. Materials Horizons: From Nature to Nanomaterials. Springer, Singapore.
- [1.1.2] Das, S., & Dhara, S. (2021). *Chemical solution synthesis for materials design and thin film device applications*. Elsevier.
- [1.1.3] *Optical thin films / products / AGC*. AGC. (n.d.).
https://www.agc.com/en/products/electronic/optical_coating/top.html
- [1.2.1] *PVD vs CVD: Differences in thin film deposition techniques*. AEM Deposition. (2023). <https://www.aemdeposition.com/blog/pvd-vs-cvd.html>
- [1.2.2] *PVD and CVD processes: What are the differences? how to choose?*. Thermi. (2024, September 26). <https://www.groupe-thermi-lyon.com/en/blog/pvd-ou-cvd/>
- [1.3.1] Kawaharamura, T., Nishinaka, H., Kamaka, Y., Masuda, Y., Lu, J.-G., & Fujita, S. (2008). Mist CVD growth of zno-based thin films and nanostructures. *Journal of the Korean Physical Society*, 53(9(5)), 2976–2980.
- [1.3.2] G. Blandenet, M. Court, Y. Lagarde Thin Layers Deposited by the Pyrosol Process *Thin Solid Films*, 77 (1981), pp. 81-90
- [1.3.3] Thin film formation technologies by mist CVD method, Takashi Shinohe (CTO& Director) FlosFIA INC.
- [1.4.1] Excitonic effects and energy upconversion in bulk and ... - diva. Linköping Studies in Science and Technology Dissertation No. 1560. (2014).

- [1.5.1] T. Onuma, S. Fujioka, T. Yamaguchi, M. Higashiwaki, K. Sasaki, T. Masui, T. Honda, *Appl. Phys. Lett.* 2013, 103, 041910.
- [1.5.2] S. J. Pearton, J. Yang, P. H. Cary IV, F. Ren, J. Kim, M. J. Tadjer, M. A. Mastro, *Appl. Phys. Rev.* 2018, 5, 011301.
- [1.5.3] H. H. Tippins, *Phys. Rev.* 1965, 140, A316.
- [1.5.4] M. Higashiwaki, K. Sasaki, A. Kuramata, T. Masui, S. Yamakoshi, *Appl. Phys. Lett.* 2012, 100, 013504.
- [1.5.5] M. Baldini, M. Albrecht, A. Fiedler, K. Irmscher, D. Klimm, R. Schewski, G. Wagner, *J. Mater. Sci.* 2016, 51, 3650.
- [1.5.6] K. Goto, K. Konishi, H. Murakami, Y. Kumagai, B. Monemar, M. Higashiwaki, A. Kuramata, S. Yamakoshi, *Thin Solid Films* 2018, 666, 182.
- [1.5.7] E. Ahmadi, O. S. Koksaldi, S. W. Kaun, Y. Oshima, D.B. Short, U. K. Mishra, J. S. Speck, *Appl. Phys. Express* 2017, 10, 041102.
- [1.5.8] Y. Zhang, F. Alema, A. Mauze, O. S. Koksaldi, R. Miller, A. Osinsky, J. S. Speck, *APL Mater.* 2019, 7, 022506.
- [1.5.9] S. Rafique, L. Han, A. T. Neal, S. Mou, J. Boeckl, H. Zhao, *phys. status solidi(a)* 2018, 215, 1700467.
- [1.5.10] H. Yang, Q. Tao, X. Zhang, A. Tang, J. Ouyang, *J. Alloys Compd.* 459 (2008) 98.
- [1.5.11] G.A. Nicklasson, C.G. Granqvist, *J. Mater. Chem.* 17 (2007) 127–156.

- [1.5.12] S. Seo, M.J. Lee, D.H. Seo, E.J. Jeoung, D.S. Suh, Y.S. Joung, I.K. Yoo, I.R. Hwang, S.H. Kim, I.S. Byun, J.S. Kim, J.S. Choi, B.S. Park, *Appl. Phys. Lett.* 85 (2004) 5655–5657.
- [1.5.13] I. Hotovy, J. Huran, P. Siciliano, S. Capone, L. Spiess, V. Rehacek, *Sens. Actuators B* 78 (2001) 126–132.
- [1.5.14] L. Ai, G. Fang, L. Yuan, N. Liu, M. Wang, C. Li, Q. Zhang, J. Li, X. Zhao, *Appl. Surf. Sci.* 254 (2008) 2401–2405.
- [1.5.15] S. Nandy, U.N. Maiti, C.K. Ghosh, K.K. Chattopadhyay, *J. Phys. Condens. Matter* 21 (2009) 115804.
- [1.5.16] K. Xerxes Steirer, J.P. Chesin, N.E. Widjonarko, J.J. Berry, A. Miedaner, D.S. Ginley, D.C. Olson, *Org. Electron.* 11 (2010) 1414–1418.
- [1.5.17] G.H. Guai, M.Y. Leiw, C.M. Ng, C.M. Li, *Adv. Energy Mater.* 2 (2012) 334–338.
- [1.5.18] J. He, H. Lindström, A. Hagfeldt, and S. E. Lindquist, *The Journal of Physical Chemistry B*, 103 (1999) 8940-8943.
- [1.5.19] G. A. Niklasson, and C. G. Granqvist, *Journal of Materials Chemistry*, 17 (2007) 127-156
- [1.5.20] J.K. Kang, S.W. Rhee, *Thin Solid Films* 391 (2001) 57–61.
- [1.5.21] H.L. Lu, G. Scarel, M. Alia, M. Fanciulli, S.J. Ding, D.W. Zhang, *Appl. Phys. Lett.* 92 (2008) 222907.
- [1.5.22] D.Y. Jiang, J.M. Qin, X. Wang, S. Gao, Q.C. Liang, J.X. Zhao, *Vacuum* 86 (2012) 1083–1086

[1.5.23] Diao, C.-C.; Huang, C.-Y.; Yang, C.-F.; Wu, C.-C. Morphological, Optical, and Electrical Properties of p-Type Nickel Oxide Thin Films by Nonvacuum Deposition. *Nanomaterials* **2020**, *10*, 636.

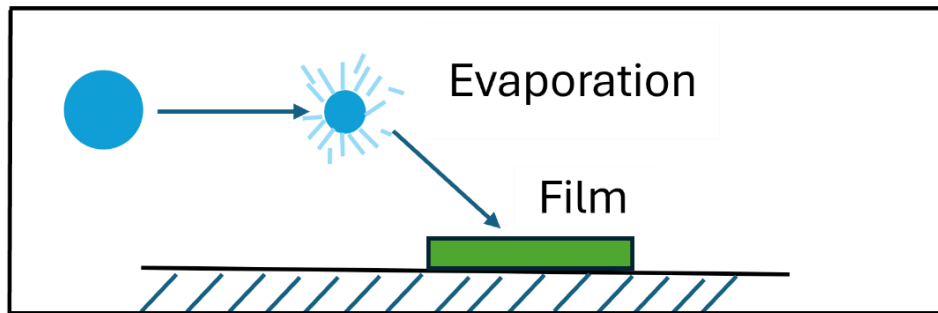
Chapter 2. Theory of mist CVD

In the previous chapter, the importance of enhancing the thin film growth process was discussed, highlighting mist CVD technology as a promising solution to the environmental and economic challenges posed by other thin film growth techniques. This chapter will delve into the mechanism of the mist CVD growth process, its characteristics, and provide a theoretical review of the mist CVD process.

2.1 Mist vs Spray

To explain the mist CVD process, understanding the mist itself is important. The term "mist" has been commonly used in daily life such as ultrasonic diffusers, humidifiers, beauty devices, etc. Mist refers to liquid droplets or their aggregates suspended in the air without any velocity. While the term spray also refers to liquid droplets, they imply applying liquid droplets by spraying. Although both refer to liquid droplets, their states differ significantly. This distinction, often overlooked, is crucial in this thesis for thin-film growth and is highly valued. The difference between mist and spray is illustrated in Figure 7.

Mist deposition



Spray deposition

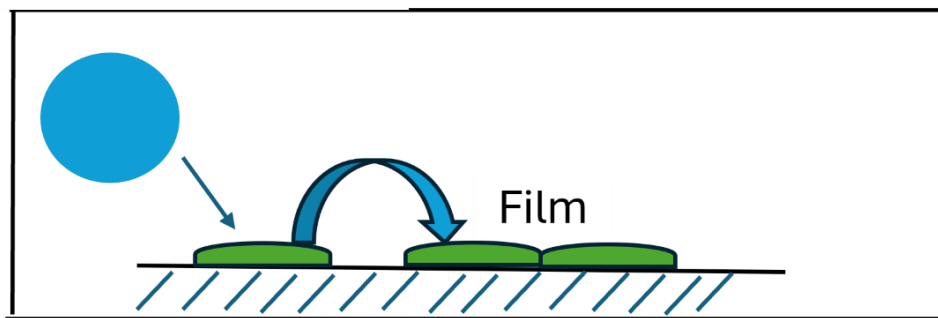


Figure 7. Mist deposition vs spray deposition

Mist deposition has the characteristics that mist has zero velocity and almost all solvents evaporate before arriving onto the substrate. This characteristic leads to flat surface films and layered structures. On the other hand, spray deposition has the characteristic that droplets directly adhere to the substrate with high velocity. This leads to limited migration on the surface and the surface tends to be rough. For this reason, mist deposition has an advantage over spray deposition because of its ability to control

2.2 Mist CVD (equipment and approach)

In the mist CVD process, a solution is made into a mist by applying ultrasound wave energy and carried by a carrier gas, and a thin film is deposited through thermal decomposition. Mist droplets produced are particularly small, so they can stay in the air, and be transported or move through laminar flow like a gas. Figure 8 shows the schematic of the mist CVD process.

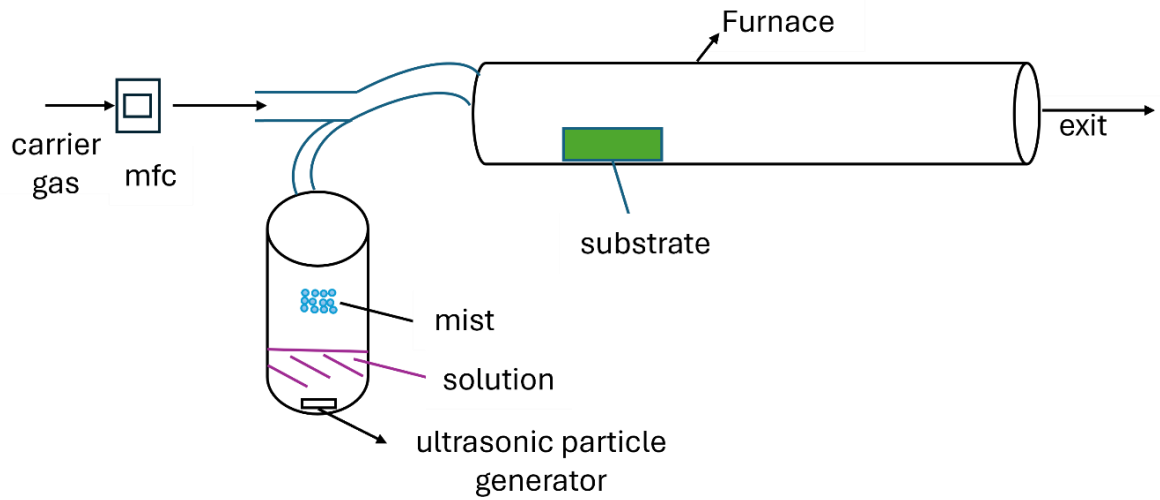


Figure 8. Schematic of mist CVD

The mist CVD technology used in this thesis employs an ultrasonic approach. This technique utilizes a piezoelectric element to atomize liquid (the propagation medium) [2.2.1]. The vibrations generated by the piezoelectric element create pressure differences in the liquid, propagating through it. Most of the vibrational energy is lost at the liquid surface, causing it to vibrate. As the vibration increases, the liquid surface is lifted, and if

the vibrations are strong enough, the surface tension is overcome, causing the liquid to split. The droplet size depends on the frequency of the surface waves, which is determined by the natural frequency of the piezoelectric element [2.2.2]. Equipment used in mist CVD is divided into two main parts: the raw material supply section and the film deposition section. Figure 8 illustrates the two main parts of the mist CVD process. The raw material supply section is responsible for atomizing the precursor solution into mist and transporting it to the deposition section using a carrier gas. In this thesis, oxygen and Ar are used for carrier gas. The film deposition section heats the transported mist to promote chemical reactions for thin film formation.

Ultrasonic particle generator as shown in Figure 8 generates mist from the solution. This method can produce uniform droplets with sizes around a few micrometers. The ultrasonic methods generate droplets with very low initial velocities, allowing the small droplets to remain suspended in the air. The explanation of the principle of ultrasonic atomization is as follows. When ultrasonic vibration energy is applied to a liquid, it creates capillary waves (capillary waves) and cavitation (cavity phenomenon) on the liquid surface or inside the liquid, with frequencies specific to the liquid. Countless capillary waves are formed on the liquid surface. When the amplitude of these waves becomes greater than the surface tension or gravity of the liquid, the liquid undergoes regular splitting, resulting in atomization of the liquid. Additionally, it has been reported that the surface tension of water decreases due to capillary waves, making it more likely to become mist-like. Various theories have been proposed for the principle of liquid atomization by ultrasonic waves [2.2.3], but the above principle is the most plausible

among them. In general, since the sound source is planar, spatial variations in sound pressure occur depending on the frequency, resulting in directionality. This allows for much more efficient sound convergence and misting than audible sound. Figure 8 also shows the schematic of the mist generator. An ultrasonic transducer forms the mist particles from a precursor solution that is mixed with a metal salt such as $\text{Ni}(\text{acac})_2$ and de-ionized water. The atomized mist is then transferred to the reactor by a carrier gas such as Ar and oxygen. In the thermal decomposition regions, the oxide layer is deposited on the surface using vaporized precursors following the ordinary CVD mechanism.

2.3 Theoretical review of Ultrasound wave

Since an ultrasonic mist generator is used in this thesis, which utilizes ultrasound waves, the theoretical review of ultrasonic sound waves is important. Ultrasonic sound waves propagate through mediums such as gases, liquids, and solids. However, it cannot travel through a vacuum as there is no medium, which is a significant difference from electromagnetic waves. One of the key characteristics of ultrasound is that it propagates better through liquids and solids than through air, unlike electromagnetic waves, which struggle in such mediums. This property of ultrasound offers valuable insights for its applications. The range of frequencies of the ultrasonic sound is shown in Figure 9.

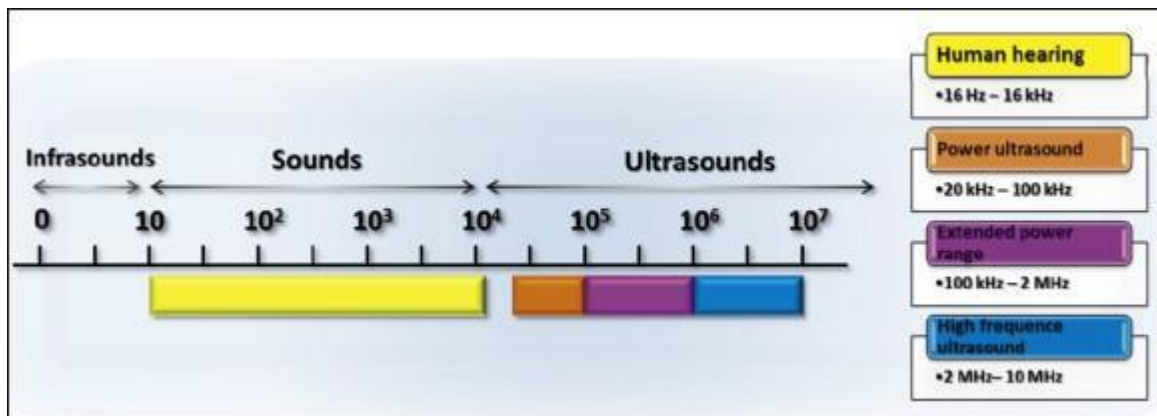


Figure 9. Range of sound [2.3.1]

Sounds of frequency above 16 kHz are referred to as ultrasounds, and sound frequencies below 16 Hz are infrasound. A sound wave is a longitudinal wave. The velocity and acceleration of ultrasonic sound waves in liquid is given in Equation 2.3.1:

$$v = \omega\mu = \sqrt{\frac{K}{\rho}} \quad 2.3.1$$

Where:

$$K = \text{bulk modulus} = \rho \frac{dp}{\rho}$$

Equilibrium density and pressure are expressed as ρ and p respectively.

Acceleration is given by Equation 2.3.2:

$$a = \omega^2 A \quad 2.3.2$$

Where:

$$\omega = 2\pi f.$$

f is the frequency.

A is the amplitude and is given by Equation 2.3.3:

$$A = \frac{1}{2\pi f} \sqrt{\frac{I}{Z_0}} \quad 2.3.3$$

Where I = intensity (W/m^2) and Z_0 = impedance of sound. As shown in Equation 2.3.2 and Figure 9, due to the high frequency of ultrasonic sound waves, their acceleration is greater compared to human-hearing sound. Unlike low-frequency human hearing sound, high-frequency sound exhibits directivity. Since the sound source is not essentially a point source, the sound waves radiated from the source interfere with each other in space, resulting in variations in sound pressure in the propagation space. This is the directivity of sound. The larger the dimensions of the sound source compared to the wavelength, the

sharper the directivity becomes. This is why using larger speakers generally improves sound quality and the sense of presence, due to this directivity. Additionally, when compared to electromagnetic waves, even the fastest sound waves have a speed of only a few thousand meters per second, so wavelengths can be shortened even at low frequencies. Therefore, compared to electromagnetic waves, sound waves can more easily achieve sharp directivity.

2.4 Theoretical review of mist particle behavior

The size of the mist particle is important as it affects the growth rate and thin film quality.

The diameter of the mist particle is given by Lang's formula which is given by Equation

2.4.1 [2.4.1]:

$$d = 0.68 \left(\frac{\pi \alpha}{\rho f^2} \right)^{\frac{1}{3}} \quad 2.4.1$$

where:

α is the surface tension.

ρ is the liquid density.

f is the frequency.

In this thesis, the frequency is set to 2.4MHz and the size of the particles is about 3 μ m. It

is noted that Lang's formula is valid up to 3MHz. Above 3MHz, it is reported that

particles do not change their size that much. The number 0.68 came from the

experimental data [2.4.1]. Kinetics of the mist particle is given by the Equation 2.4.2

[2.4.2]:

$$\frac{\pi}{6} d^3 \rho \frac{av}{dt} = \frac{\sigma \eta g^u}{C_c} (\vec{u} - v) + \frac{\pi}{6} d^3 \rho \frac{au}{g dt} + \frac{\pi}{12} d^3 \rho \left(\frac{au}{g dt} - \frac{av}{dt} \right) + \quad 2.4.2$$

$$\frac{3}{2} d^2 (\pi \rho \eta)^{\frac{1}{2}} \int_{t_0}^t \left[\frac{d\vec{u}}{dt'} - \frac{dv}{dt'} \right] \frac{dt'}{(t-t')^{\frac{1}{2}}} + \vec{F}_E + \vec{F}_{NU}$$

Where:

d is the diameter of the particle.

v is the velocity vector.

u is the fluid velocity vector.

ρ is the density of the particle.

ρ_g is the density of the fluid.

η_g is the viscosity of the fluid.

F_E is the external force.

F_{NU} is the external forces that cause motion due to the heterogeneity of the medium.

C_c is the Cunningham correction factor, and it is a dimensionless number representing the degree of gas dilution, which is expressed as a function of the Knudsen coefficient. C_c is given by Equation 2.4.3 [2.4.2]:

$$C_c = 1 + Kn\{1.257 + 0.4\exp\left(\frac{-1.1}{Kn}\right)\}$$

Where $Kn = \frac{\lambda_g}{d}$ is the Knudsen coefficient.

The left side of the Equation 2.4.2 represents inertia. The representation of the right side of Equation 2.4.2 is as follows:

1st order = fluid resistance.

2nd order = The force acting when particles accelerate or decelerate a fluid.

3rd order = The force associated with the acceleration or deceleration of the apparent mass of particles.

4th order = The Basset term represents the change in total momentum gained by the fluid when particles are accelerated.

5th order = external force such as gravity.

6th order = external forces that cause motion due to the heterogeneity of the medium, such as Brownian motion or migration.

When $u = 0$, $t = 0$, and $v = 0$ (stationary condition under gravity), the 4th order (Basset term) can be ignored since it is stationary. Particle starts to fall due to gravity and the motion is one-dimensional (gravity force). External force is given by Equation 2.4.3:

$$F_E = m\left(1 - \frac{\rho_g}{\rho}\right)g \quad 2.4.3$$

Where $(1 - \rho_g/\rho)$ represents surrounding fluids).

By assuming the particle is spherical, mass is given by Equation 2.4.4:

$$m' = m \left(1 - \frac{\rho_g}{2\rho}\right) \quad 2.4.4$$

Where:

m' is the apparent mass. The apparent mass of particles is influenced as if they were subjected to only half the mass of the fluid displaced by the sphere.

Now Equation 2.4.2 simplifies to Equation 2.4.5:

$$\frac{dv}{dt} = \frac{3\rho_g v^2 C_D}{4(\rho + \rho_g) d C_c} \frac{(\rho + \rho_g)g}{(\rho + \rho_g/2)} \quad 2.4.5$$

By using τ (tow), (saturation time of the velocity of the particle) Equation 2.4.5 is further simplified to Equation 2.4.6.:

$$\frac{dv}{dt} \frac{1}{\tau} v = \frac{(\rho + \rho_g)g}{(\rho + \rho_g/2)} \quad 2.4.6$$

Where $\tau = \frac{d^2(\rho + \rho_g/2)C_c}{18\eta}$ is the saturation time.

Using Equation 2.4.6, the saturation time and velocity of the particle due to gravity can be obtained. It is important to determine the flow rate of the carrier gas by considering the above equation since the factor of the deposition rate of the thin film is known to depend on the substrate temperature and flow rate.

Reference

[2.2.1] W.R. Wood and A.L. Loomis, "The Physical and Biological Effects of High Frequency Sound Wave of Great Intensity", *Philos. Mag.*, (1927) pp.417-437.

[2.2.2] G. Blandenet, M. Court, and Y. Lagarde, "Thin layers deposited by the pyrosol process", *Thin Solid Films*, Vol.77 (1981) pp.81-90.

[2.2.3] Chika Chiba, "Ultrasonic Spray", Sankaido (1990)

[2.3.1] Mechanical wave. *Mechanical Wave - an overview* | ScienceDirect Topics. (n.d.).

<https://www.sciencedirect.com/topics/chemistry/mechanical-wave>

[2.4.1] R.J. Long, "Ultrasonic Atomization of Liquids", *J. Acoustical Soc. Amer.*, Vol.34 (1962) pp.6-8.

[2.4.2] Kikuo Okuyama, "Particle Engineering", Ohmsha Publishing Bureau (1992)

Chapter 3 Characterization method

In this thesis, XRD (X-ray diffraction), Hall effect measurements, and SEM (scanning electron microscope) are used to determine the characteristics of the NiO thin film.

3.1 X-ray diffraction (XRD)

X-ray diffraction (XRD) is a common measurement method used to evaluate the crystal structure of thin films. It is also known as X-ray crystallography. This measurement technique determines how atoms are arranged within the crystal. Inside the crystal, atoms are periodically and regularly arranged, forming a spatial lattice with intervals going from several angstroms to several nanometers. When X-rays, electromagnetic waves with wavelengths of about 1 pm to 10 nm, are incident, the crystal lattice diffracts and scatters the X-rays. The scattered X-rays interfere with each other, reinforcing waves in specific directions. By detecting these diffracted X-rays with a detector, the crystal structure of the sample can be examined. Figure 10 shows the necessary conditions for the occurrence of constructive interference.

Bragg's law

$$\lambda = 2d_{hkl} \sin \Theta_B$$

Necessary condition for
constructive interference
(light coherence)

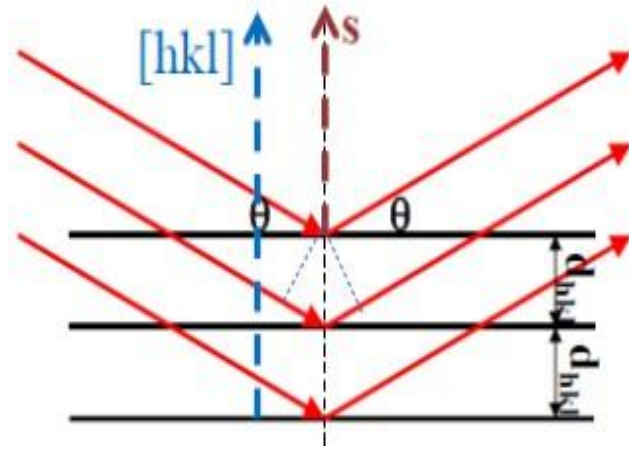
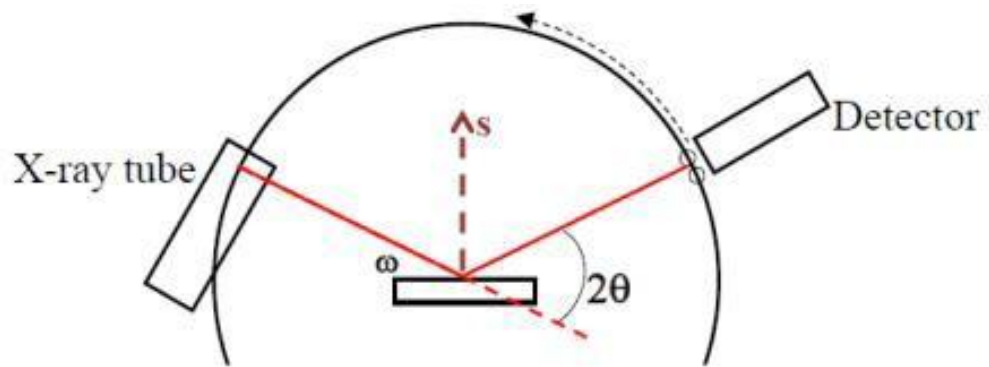


Figure 10. Bragg's law

When X-rays are incident on a crystal with a spacing of d , as shown in Figure 10, the waves interfere and reinforce each other when the angle of incidence and reflection match a certain angle. This condition, known as Bragg's law, occurs when X-rays of a specific wavelength strike a crystal at particular angles, causing the scattered X-rays to interfere constructively and produce a strong reflected beam. The equation for describing Bragg's law is given by Equation 3.1.1:

$$2d \sin \theta = n\lambda \quad 3.1.1$$

When Equation 3.1.1 meets, the scattered light interferes constructively, allowing the diffracted light to be observed. In this thesis, an omega-2theta scan is used as shown in Figure 11.



- The incident angle (ω) is defined between the X-ray source and the sample.
- The diffracted angle, 2θ , is defined between the incident beam and detector angle.

Figure 11. Omega-2theta scan

3.2 Hall effect measurement

Hall effect measurement is also a common measurement method that utilizes the Hall effect. The Hall effect is a consequence of the forces that are exerted on moving charges by electric and magnetic fields [3.2.1]. By applying a current and a magnetic field to a sample, the resistivity, carrier density, and Hall mobility can be extracted. Figure 12 shows the schematic of the Hall effect measurement.

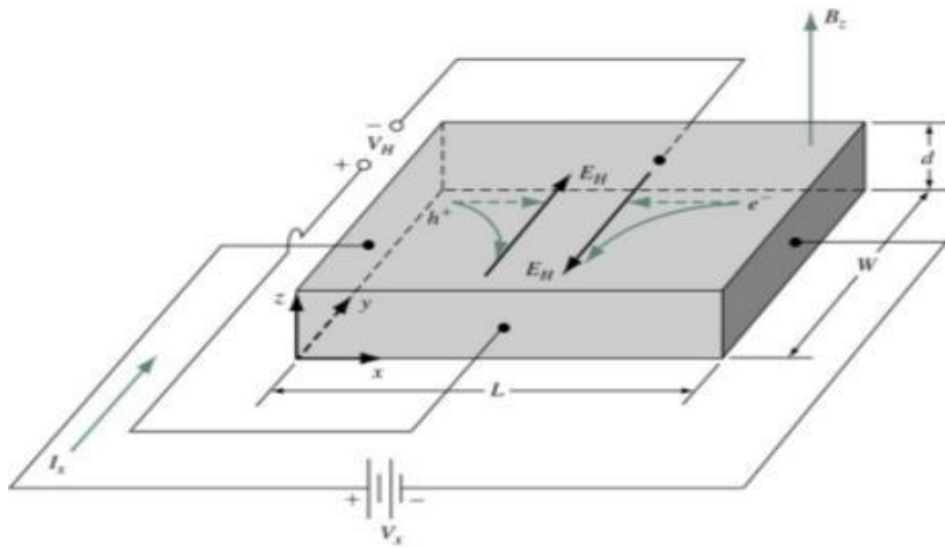


Figure 12. Hall effect measurement [3.2.1]

When the carrier of charge, q , moves with velocity, v , in a magnetic field, B , where v is in the x direction and B is in the z direction in Figure 12, Lorentz force will exert as shown in Figure 12. The equation of the Lorentz force is given by Equation 3.2.1:

$$F = qv \times B \quad 3.2.1$$

Where:

F is the force.

q is the electron charge.

v is the drift velocity.

B is the magnetic field.

When the carrier of charge is in an electric field, E, the total force is given by Equation

3.2.2:

$$F = qE + qVB \quad 3.2.2$$

Where:

E is the electric field.

V is the Hall Voltage.

The induced electric field in the y direction is called the Hall field and produces Hall

Voltage. The equation is given by 3.2.3:

$$V = EW = vBW \quad 3.2.3$$

Where:

W is the width of the sample.

v is the drift velocity. For p-type semiconductor, the drift velocity of holes is given by Equation 3.2.4:

$$v = J/qp = I/qp(Wd) \quad 3.2.4$$

Where:

J is the current density.

p is the hole concentration.

d is the thickness of the sample.

By substituting the Equation 3.2.4 into the Equation 3.2.3, Equation 3.2.3 becomes

Equation 3.2.5:

$$V = I \cdot B / (qpd) \quad 3.2.5$$

From the Equation 3.2.5, hole concentration is given by Equation 3.2.6:

$$p = I \cdot B / (qdV) \quad 3.2.6$$

For p-type semiconductors, the current density is given by Equation 3.2.7:

$$J = qp\mu E \quad 3.2.7$$

From Equation 3.2.7, hole mobility is given by Equation 3.2.8:

$$\mu = IL / (qpVWd) \quad 3.2.8$$

The details of the derivation of Equation [3.2.1-3.2.8] can be found [3.2.2]. In this thesis, the Ecopia Hall effect measurement system is used for NiO characterization.

3.3 Surface morphology characterization via SEM

Electron microscopes are mainly divided into two types: Transmission Electron Microscopes (TEM) and Scanning Electron Microscopes (SEM). In recent years, the Scanning Transmission Electron Microscope (STEM) has also garnered attention and was used as one of the methods to evaluate thin films. In this thesis, SEM is used to check the surface morphology of NiO thin film. SEM focuses on an electron beam generated from an electron source and scans it in two dimensions over the sample to obtain images from the signals generated. When the electron beam is irradiated in a vacuum, it generates signals such as Secondary Electrons (SE), Backscattered Electrons (BSE), X-rays, fluorescence, and absorbed electrons as shown in Figure 13. SE provides surface information, BSE provides compositional information, and X-rays provide elemental information. By imaging these signals, detailed images can be obtained, allowing the observation of the structures of the thin film.

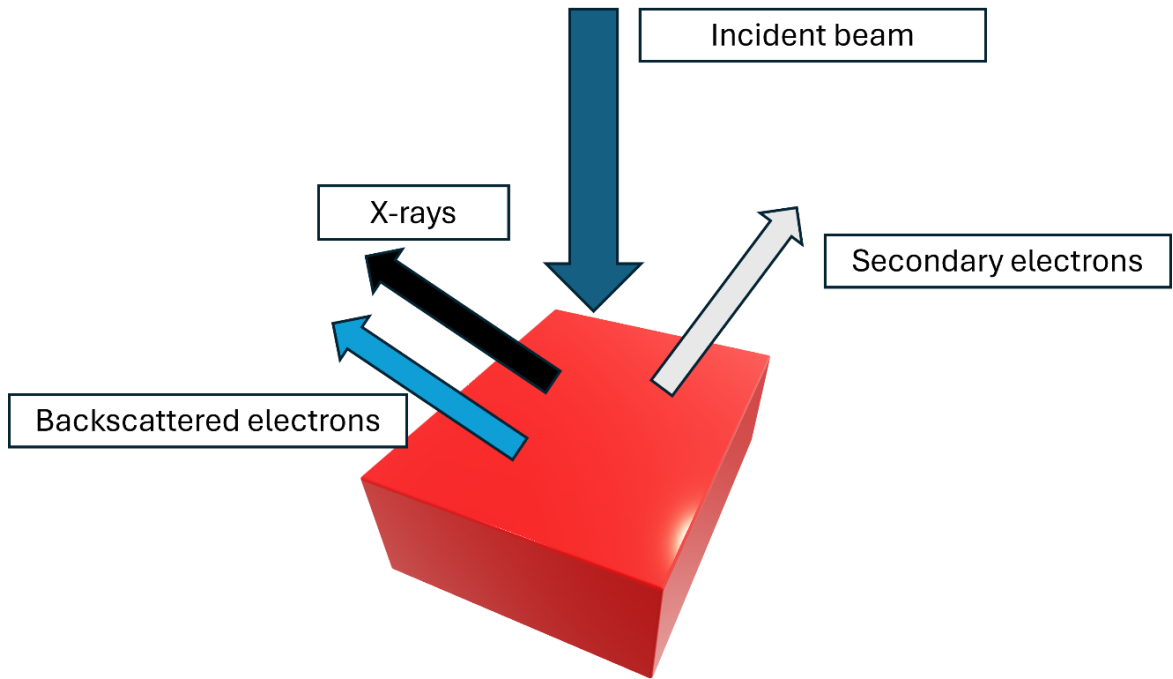


Figure 13. Schematic of SEM image

3.4 X-ray Photoelectron Spectroscopy (XPS)

XPS is a technique for analyzing a material's surface chemistry. XPS can measure elemental composition as well as the chemical and electronic state of the atoms within a material [3.4.1]. XPS utilizes the photoelectric effect. In this method, X-rays are directed at the surface of a sample, causing the emission of photoelectrons from the material. By measuring the kinetic energy of these emitted photoelectrons, it can determine the elemental composition, chemical state, and electronic state of the atoms within the top layers of the material. The theory of the photoelectric effect is shown in Figure 14.

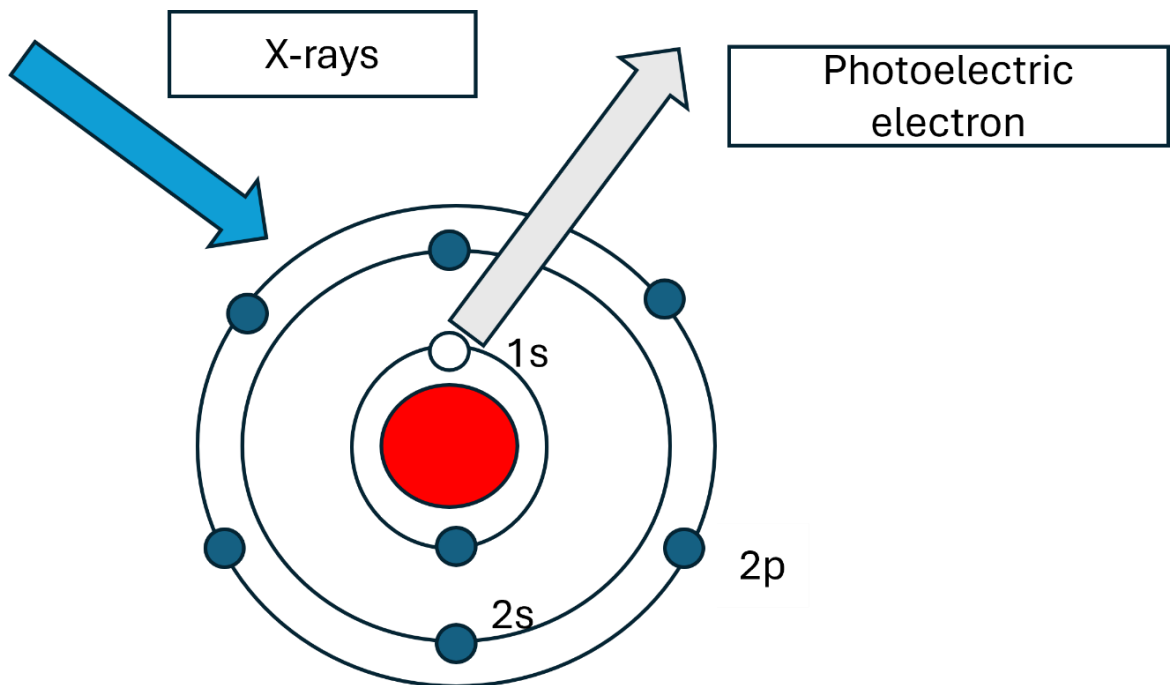


Figure 14. XPS theory

By measuring the kinetic energy of photoelectrons emitted from the solid surface due to X-ray excitation, it is possible to observe the energy change associated with the transition from the ground state to the excited state in the photoemission process. In the photoemission process, the energy change associated with the transition from the ground state to the excited state can be observed. This transition occurs when an electron absorbs the energy from an incoming X-ray photon, leading to its ejection from the atom. The X-ray must be low energy and have less transmission to be used in XPS measurement. Aluminum (Al $K\alpha$) and Magnesium (Mg $K\alpha$) are commonly used as X-ray sources in XPS due to their suitable energy levels [3.4.2]. Figure 15 shows the mechanism of photoelectron generation.

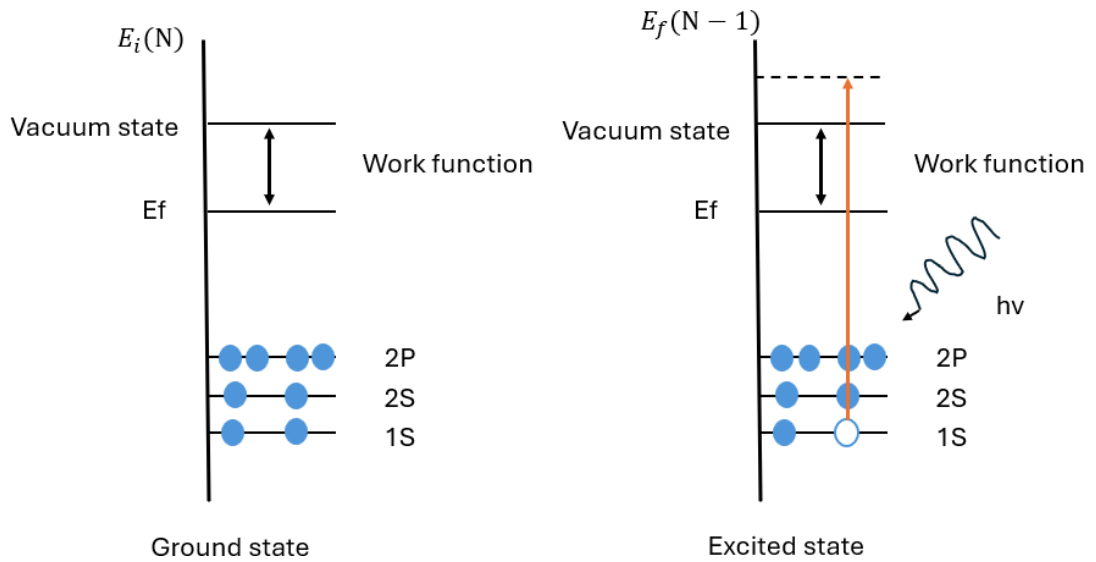


Figure 15. Mechanism of photoelectron generation

From the conservation of energy principle, Equation 3.4.1 can be obtained [3.4.3]:

$$E_i(N) + h\nu = E_k + E_f(N - 1) \quad 3.4.1$$

Where:

$E_i(N)$ is the energy of the first state.

$h\nu$ is the energy of the light.

$E_f(N - 1)$ is the energy of the final state.

E_k is the energy of the photoelectron.

The binding energy, E_B , can be defined by subtracting the energy of the first state from the energy of the final state. Binding energy is given by Equation 3.4.2:

$$E_f(N - 1) - E_i(N) = E_B \quad 3.4.2$$

The kinetic energy of photoelectrons in a vacuum, E'_k , is given by Equation 3.4.3:

$$E'_k = E_k - W \quad 3.4.3$$

Where:

W is the known work function of the atom.

By substituting Equation 3.4.2 and Equation 3.4.3 into Equation 3.4.1, Equation 3.4.4 can be obtained:

$$E_B = h\nu - E'_k - W \quad 3.4.4$$

Where:

$E'_k = E_k - W$ is the measurement result from the XPS.

W is the known work function of the atom.

$h\nu$ is the known energy from the X-ray source.

While SEM can also provide information about the composition of a material, it uses a different type of beam that has greater penetration depth compared to the X-ray beam used in XPS. Because of this, XPS is superior for extracting detailed surface information, making it a more suitable technique for analyzing surface chemistry and detecting thin surface layers.

Reference

[3.2.1] Semiconductor Physics and Devices Basic Principles Donal A. Neamen Fourth Edition Pg180

[3.2.2] Semiconductor Physics and Devices Basic Principles Donal A. Neamen Fourth Edition Pg180-Pg182

[3.4.1] *X-ray photoelectron spectroscopy: Learning center: Thermo fisher scientific - US.* (n.d.). <https://www.thermofisher.com/jp/ja/home/materials-science/learning-center/surface-analysis.html>

[3.4.2] X-ray photoelectron spectroscopy: XPS X-ray sources: Thermo Fisher Scientific - US. (n.d.). <https://www.thermofisher.com/jp/ja/home/materials-science/learning-center/surface-analysis/x-ray>

[3.4.3] Sugiyama, H. (2021). Fundamental of XPS.

<https://www.youtube.com/watch?v=RSHInSRUHos&t=784s>

Chapter 4 NiO growth

4.1 Mist CVD process setup

To grow NiO thin film, an original mist CVD setup is built as described in the schematic in Figure 8. The experimental setup used in this thesis is shown in Figure 16.

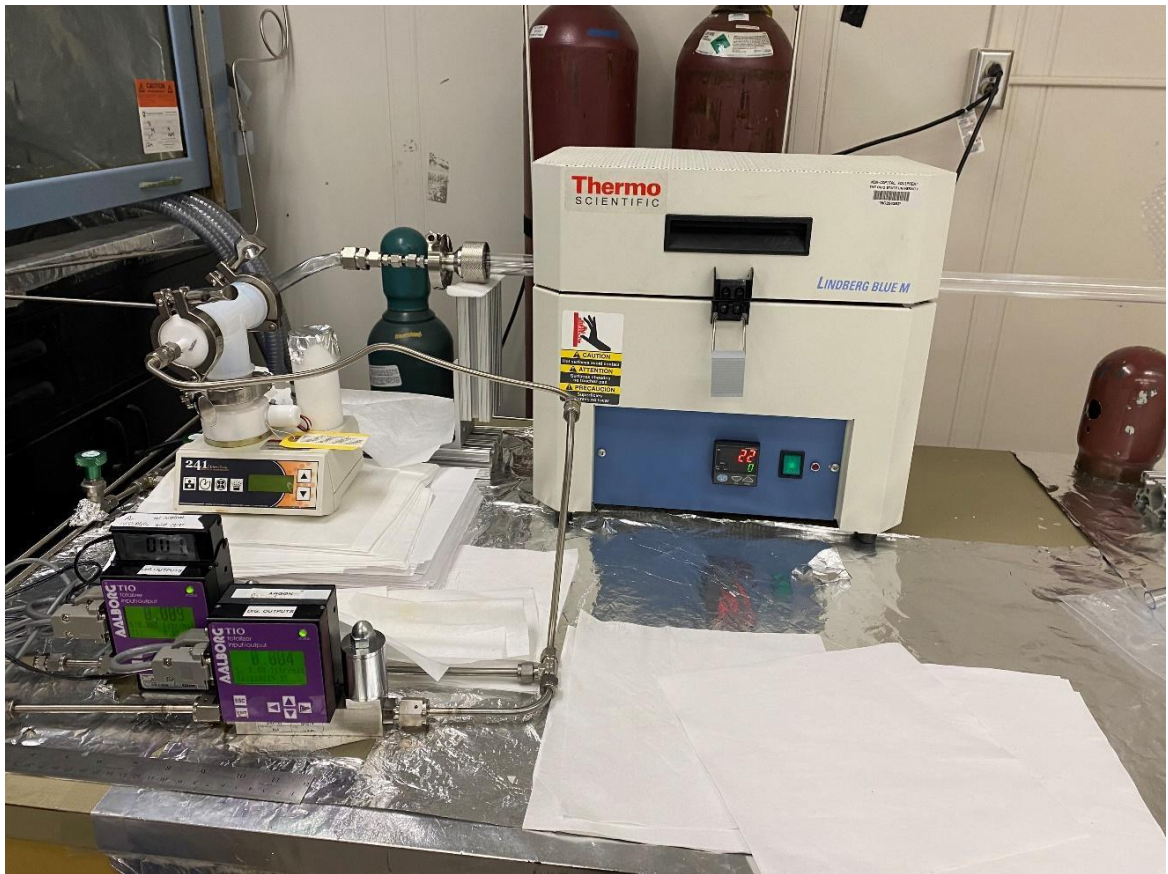


Figure 16. Experimental setup

As shown in Figure 16, two mass flow controllers are used for Ar and oxygen as the carrier gases. The main equipment, as illustrated in Figure 16, used in this thesis is listed in Table 1.

Equipment	Maker
Ultrasonic particle generator	Ultrasonic 241PGT Particle Generator makes Micron and Sub-Micron Droplets
Two mass flow controllers	Aalborg Totalizer For Gas Mass Flowmeters And Controllers With Input And Output
Furnace	Thermo Scientific Lindberg/Blue M Mini-Mite Tube Furnace with A Controller, 120V

Table 1. The main equipment used in this thesis

4.2 Growth conditions/procedure

The growth condition used in this thesis is summarized in Tale 2.

Substrate	c-sapphire
Nickle source	0.308 g Ni(acac) ₂ 96%
Solution concentration	0.02M
Solvent	EDA (1mL) + H ₂ O (60mL)
Growth temperature(C)	700
Growth time(hr)	1
Carrier gas flow rate	Ar (3L/min) and Oxygen (0.2L/min)
Water carrier to stream distance	5 cm

Table 2. NiO growth condition

C-plane sapphire substrates are used in this thesis. EDA, Ethylenediamine, is added for better resolution. The growth temperature is set to 700 degrees Celsius. A wafer carrier is put on the furnace. It has four positions to place each substrate as shown in Figure 17.



Figure 17. Wafer carrier

4.3 Result

The Ecopia hall measurement result shows that the sample is insulating. Therefore, carrier concentration, mobility, and conductivity of the NiO thin film are not obtained.

Figure 18 shows the XRD result from position 1 of the wafer carrier grown according to the Table 2 condition.

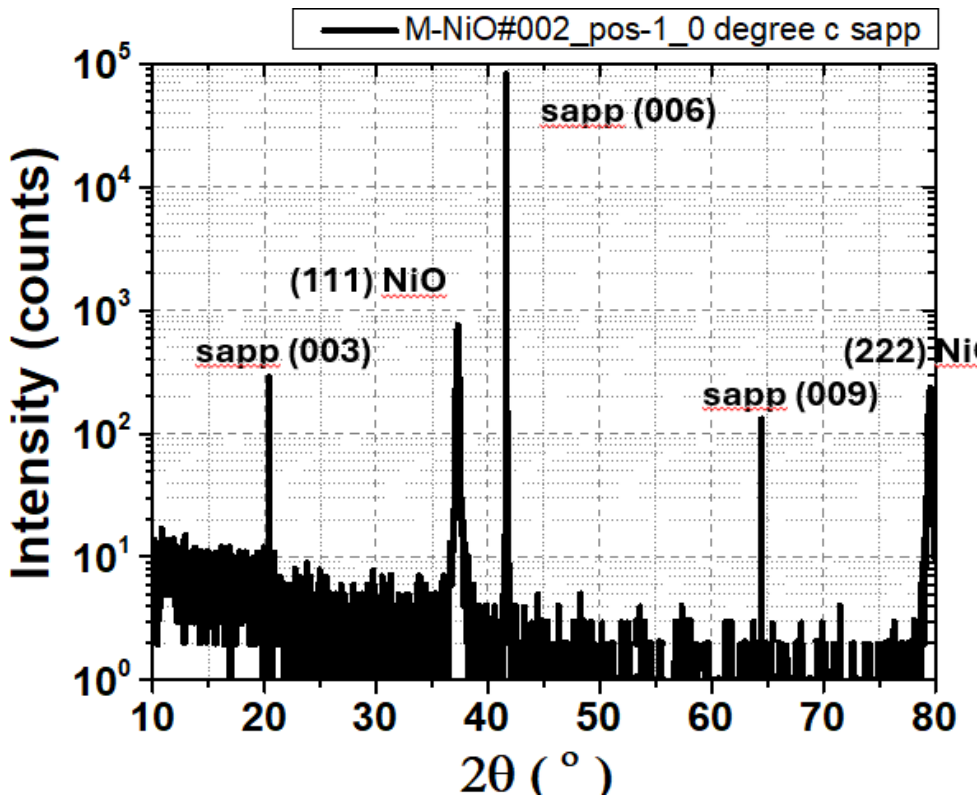


Figure 18. XRD result

The vertical axis represents intensity, and the horizontal axis represents 2θ . The measurement conditions were set to $2\theta/\omega$ targeting the thin film. The sample shows that a peak derived from NiO(111) was successfully detected. The SEM images of the sample corresponding to positions 1 and 2 are shown in Figure 19 and Figure 20.

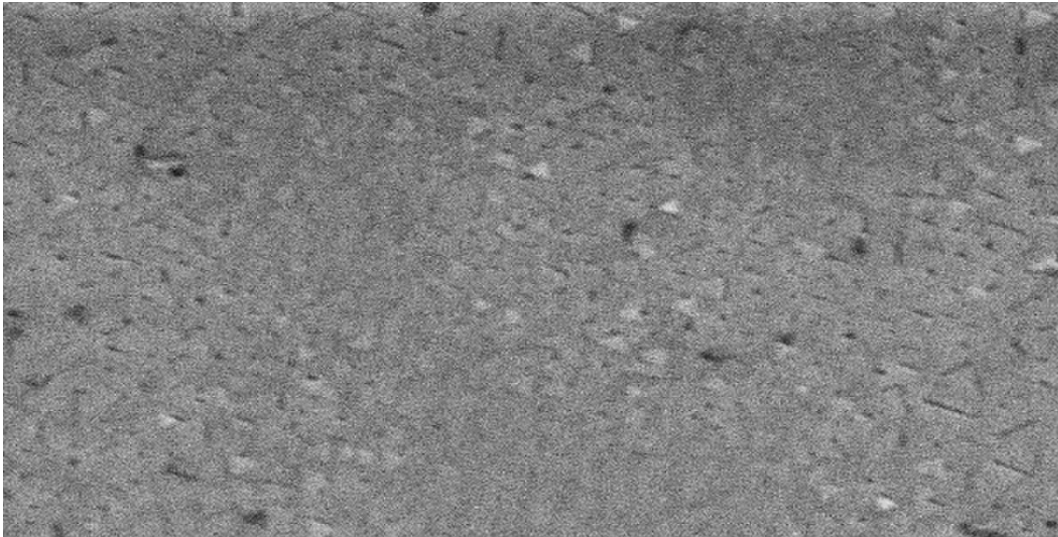


Figure 19. SEM position 1

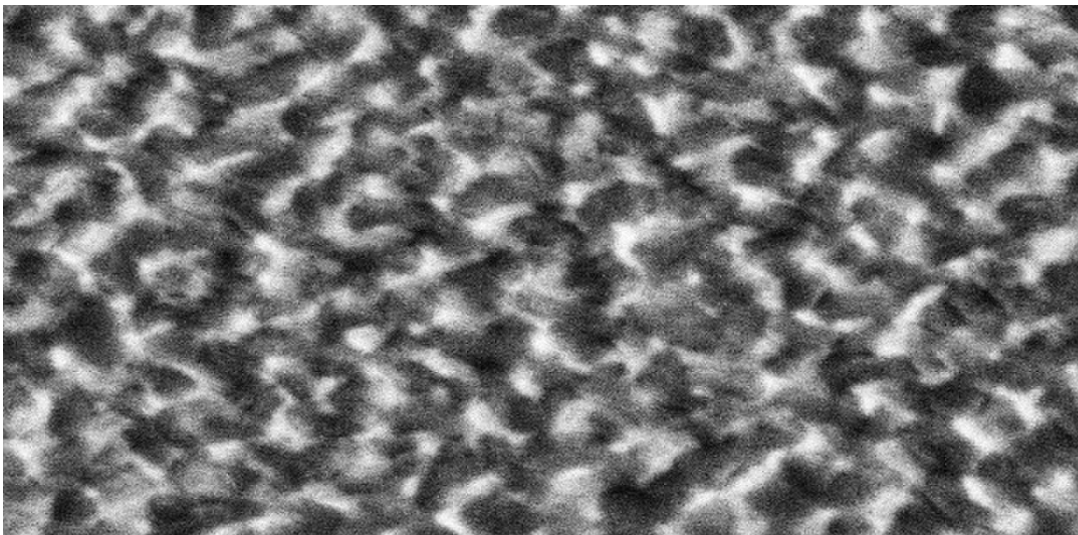


Figure 20. SEM position 2

By comparing Figure 19 and Figure 20, Figure 20 shows that the surface becomes rough as the position changes. This indicates that thin film is not deposited uniformly.

XPS result is shown in Figure 21.

	Ni % (Ni 2p)	O %	Al % (Al 2p)
pos-1	44.32	55.68	0
pos-2	15.04	26.70	58.26
pos-3	11.40	34.65	53.95
pos-4	8.66	39.68	51.66

Figure 21. XPS result

The XPS measurement result shows that nickel composition decreases as the position increases. This indicates that the deposition rate of nickel decreases therefore thickness of the thin film also decreases. Figure 21 shows that positions two, three, and four have an aluminum composition. This aluminum composition came from the X-ray source from the XPS measurement. Since the thickness of positions two, three, and four are too thin, which is not measurable as it is too thin (must be below 50nm), the Al composition had been obtained.

Chapter 5 Conclusion and Future Work

In this thesis, the mist CVD process's mechanism is discussed and NiO thin film's growth is successfully observed. XRD, XPS, and SEM results ensured NiO thin film was grown on the c-sapphire substrate. The main challenge encountered in this thesis is the lack of p-type conductivity and uniform deposition of the sample. The possible future work for this topic is: achieving p-type conductivity of NiO thin film, higher growth rate, and uniformity of thin film deposition. If uniformity and higher growth rate of NiO thin film growth might be achieved by changing the design of the mist CVD, that might lead to the commercial usage of the mist CVD process. It is also interesting to build the simulation for the mist CVD process by using the equations described in section 2.3 and 2.4.

Bibliography

- [1.1.1] Kumar, S., Aswal, D.K. (2020). Thin Film and Significance of Its Thickness. In: Kumar, S., Aswal, D. (eds) Recent Advances in Thin Films. Materials Horizons: From Nature to Nanomaterials. Springer, Singapore.
- [1.1.2] Das, S., & Dhara, S. (2021). *Chemical solution synthesis for materials design and thin film device applications*. Elsevier.
- [1.1.3] *Optical thin films / products / AGC*. AGC. (n.d.).
https://www.agc.com/en/products/electronic/optical_coating/top.html
- [1.2.1] *PVD vs CVD: Differences in thin film deposition techniques*. AEM Deposition. (2023). <https://www.aemdeposition.com/blog/pvd-vs-cvd.html>
- [1.2.2] *PVD and CVD processes: What are the differences? how to choose?* Thermi. (2024, September 26). <https://www.groupe-thermi-lyon.com/en/blog/pvd-ou-cvd/>
- [1.3.1] Kawaharamura, T., Nishinaka, H., Kamaka, Y., Masuda, Y., Lu, J.-G., & Fujita, S. (2008). Mist CVD growth of zno-based thin films and nanostructures. *Journal of the Korean Physical Society*, 53(9(5)), 2976–2980.
- [1.3.2] G. Blandenet, M. Court, Y. Lagarde Thin Layers Deposited by the Pyrosol Process *Thin Solid Films*, 77 (1981), pp. 81-90
- [1.3.3] Thin film formation technologies by mist CVD method, Takashi Shinohe (CTO& Director) FlosFIA INC.
- [1.4.1] Excitonic effects and energy upconversion in bulk and ... - diva. Linköping Studies in Science and Technology Dissertation No. 1560. (2014).

- [1.5.1] T. Onuma, S. Fujioka, T. Yamaguchi, M. Higashiwaki, K. Sasaki, T. Masui, T. Honda, *Appl. Phys. Lett.* 2013, 103, 041910.
- [1.5.2] S. J. Pearton, J. Yang, P. H. Cary IV, F. Ren, J. Kim, M. J. Tadjer, M. A. Mastro, *Appl. Phys. Rev.* 2018, 5, 011301.
- [1.5.3] H. H. Tippins, *Phys. Rev.* 1965, 140, A316.
- [1.5.4] M. Higashiwaki, K. Sasaki, A. Kuramata, T. Masui, S. Yamakoshi, *Appl. Phys. Lett.* 2012, 100, 013504.
- [1.5.5] M. Baldini, M. Albrecht, A. Fiedler, K. Irmscher, D. Klimm, R. Schewski, G. Wagner, *J. Mater. Sci.* 2016, 51, 3650.
- [1.5.6] K. Goto, K. Konishi, H. Murakami, Y. Kumagai, B. Monemar, M. Higashiwaki, A. Kuramata, S. Yamakoshi, *Thin Solid Films* 2018, 666, 182.
- [1.5.7] E. Ahmadi, O. S. Koksaldi, S. W. Kaun, Y. Oshima, D.B. Short, U. K. Mishra, J. S. Speck, *Appl. Phys. Express* 2017, 10, 041102.
- [1.5.8] Y. Zhang, F. Alema, A. Mauze, O. S. Koksaldi, R. Miller, A. Osinsky, J. S. Speck, *APL Mater.* 2019, 7, 022506.
- [1.5.9] S. Rafique, L. Han, A. T. Neal, S. Mou, J. Boeckl, H. Zhao, *phys. status solidi(a)* 2018, 215, 1700467.
- [1.5.10] H. Yang, Q. Tao, X. Zhang, A. Tang, J. Ouyang, *J. Alloys Compd.* 459 (2008) 98.
- [1.5.11] G.A. Nicklasson, C.G. Granqvist, *J. Mater. Chem.* 17 (2007) 127–156.

- [1.5.12] S. Seo, M.J. Lee, D.H. Seo, E.J. Jeoung, D.S. Suh, Y.S. Joung, I.K. Yoo, I.R. Hwang, S.H. Kim, I.S. Byun, J.S. Kim, J.S. Choi, B.S. Park, *Appl. Phys. Lett.* 85 (2004) 5655–5657.
- [1.5.13] I. Hotovy, J. Huran, P. Siciliano, S. Capone, L. Spiess, V. Rehacek, *Sens. Actuators B* 78 (2001) 126–132.
- [1.5.14] L. Ai, G. Fang, L. Yuan, N. Liu, M. Wang, C. Li, Q. Zhang, J. Li, X. Zhao, *Appl. Surf. Sci.* 254 (2008) 2401–2405.
- [1.5.15] S. Nandy, U.N. Maiti, C.K. Ghosh, K.K. Chattopadhyay, *J. Phys. Condens. Matter* 21 (2009) 115804.
- [1.5.16] K. Xerxes Steirer, J.P. Chesin, N.E. Widjonarko, J.J. Berry, A. Miedaner, D.S. Ginley, D.C. Olson, *Org. Electron.* 11 (2010) 1414–1418.
- [1.5.17] G.H. Guai, M.Y. Leiw, C.M. Ng, C.M. Li, *Adv. Energy Mater.* 2 (2012) 334–338.
- [1.5.18] J. He, H. Lindström, A. Hagfeldt, and S. E. Lindquist, *The Journal of Physical Chemistry B*, 103 (1999) 8940-8943.
- [1.5.19] G. A. Niklasson, and C. G. Granqvist, *Journal of Materials Chemistry*, 17 (2007) 127-156
- [1.5.20] J.K. Kang, S.W. Rhee, *Thin Solid Films* 391 (2001) 57–61.
- [1.5.21] H.L. Lu, G. Scarel, M. Alia, M. Fanciulli, S.J. Ding, D.W. Zhang, *Appl. Phys. Lett.* 92 (2008) 222907.
- [1.5.22] D.Y. Jiang, J.M. Qin, X. Wang, S. Gao, Q.C. Liang, J.X. Zhao, *Vacuum* 86 (2012) 1083–1086

- [1.5.23] Diao, C.-C.; Huang, C.-Y.; Yang, C.-F.; Wu, C.-C. Morphological, Optical, and Electrical Properties of p-Type Nickel Oxide Thin Films by Nonvacuum Deposition. *Nanomaterials* **2020**, *10*, 636.
- [2.2.1] W.R. Wood and A.L. Loomis, "The Physical and Biological Effects of High Frequency Sound Wave of Great Intensity", *Philos. Mag.*, (1927) pp.417-437.
- [2.2.2] G. Blandenet, M. Court, and Y. Lagarde, "Thin layers deposited by the pyrosol process", *Thin Solid Films*, Vol.77 (1981) pp.81-90.
- [2.2.3] Chika Chiba, "Ultrasonic Spray", Sankaido (1990)
- [2.3.1] Mechanical wave. *Mechanical Wave - an overview | ScienceDirect Topics*. (n.d.). <https://www.sciencedirect.com/topics/chemistry/mechanical-wave>
- [2.4.1] R.J. Long, "Ultrasonic Atomization of Liquids", *J. Acoustical Soc. Amer.*, Vol.34 (1962) pp.6-8.
- [2.4.2] Kikuo Okuyama, "Particle Engineering", Ohmsha Publishing Bureau (1992)
- [3.2.1] *Semiconductor Physics and Devices Basic Principles* Donal A. Neamen Fourth Edition Pg180
- [3.2.2] *Semiconductor Physics and Devices Basic Principles* Donal A. Neamen Fourth Edition Pg180-Pg182
- [3.4.1] *X-ray photoelectron spectroscopy: Learning center: Thermo fisher scientific - US*. (n.d.). <https://www.thermofisher.com/jp/ja/home/materials-science/learning-center/surface-analysis.html>

[3.4.2] X-ray photoelectron spectroscopy: XPS X-ray sources: Thermo Fisher Scientific
- US. (n.d.). <https://www.thermofisher.com/jp/ja/home/materials-science/learning-center/surface-analysis/x-ray>

[3.4.3] Sugiyama, H. (2021). Fundamental of XPS.

<https://www.youtube.com/watch?v=RSHInSRUHos&t=784s>